Contribution from the Laboratorium für Anorganische Chemie, ETH-Zentrum, CH-8092 Zürich, Switzerland

Structures of Some $HgX_2(PPh_3)_2$ Complexes As Studied by ^{31}P NMR, X-ray, and Extended-Hückel Molecular Orbital Methods

H. B. BUERGI,* R. W. KUNZ, and P. S. PREGOSIN*

Received January 24, 1980

The complexes $HgX_2(PPh_3)_2$, X = NO_3, Cl, Br, SCN, I, and CN, have been studied with the use of ^{31}P NMR techniques. X-ray structural data for the NO_3 and CN compounds are reported. The solution and solid-state measurements reveal a marked distortion of these molecules from idealized tetrahedral geometry: larger $^1J(^{199}Hg,^{31}P)$ coupling constants and P–Hg–P bond angles are found for the harder X ligands than for the softer ones. Values of $^1J(^{199}Hg,^{31}P)$ have been calculated by using extended-Hückel methods. The trends obtained from the calculations are in accord with the experimental findings and suggest that the anion, X, and the P–Hg–P angle make important contributions to the changes in $^1J(^{199}Hg,^{31}P)$. ^{31}P NMR data for the complexes HgI_2P_2, P = $P(m\text{-}CF_3C_6H_4)_3$, PPh_3, $PPh_2(CH_2Ph)$, $(Ph_2PCH_2CH_2)_2S$, PPh-*n*-Bu_2, P-*n*-Bu_3, and P(c-Hx)$_3$, are also reported.

Introduction

We have recently reported[1] that the one-bond silver–phosphorus coupling constant, $^1J(^{107}Ag,^{31}P)$, in conjunction with other physical data, provides a useful probe for changes in molecular structure in solution. Thus in the molecule AgI(PP) (PP = 2,11-bis((diphenylphosphino)methyl)benzo[*c*]phenanthrene), the silver–phosphorus coupling suggests a structure in which the silver is three-coordinate with the ligand atoms disposed in a distorted trigonal-planar arrangement about the metal. On the other hand the value of $^1J(Ag,P)$ for $Ag(NO_3)(PP)$ is more in keeping with an approximate "*T*" arrangement for the metal, oxygen, and phosphorus atoms. The existence of both donor atom geometries has been confirmed in the solid state by X-ray structure analysis of CuClPP·PhCN, AgClPP, and AuClPP.[2]

As an extension of this type of study we have begun a consideration of the effect of the ligand X in the complexes $HgX_2(PPh_3)_2$ on their solution and solid-state molecular structures. These molecules are especially suitable for study in solution via ^{31}P nuclear magnetic resonance (NMR) since mercury possesses an isotope with nuclear spin $I = {}^1/_2$ (^{199}Hg, natural abundance = 16.8%) and a relatively large magnetic moment. Thus, the magnitude of $^1J(Hg,P)$ should be sufficiently large to mirror any significant change in the structure of the complex. There have been several reports concerned with the ^{31}P NMR parameters of mercury–phosphine complexes which have shown that $^1J(Hg,P)$ is sensitive to structural changes (e.g., $^1J(Hg,P)$ for $HgCl_2(P\text{-}n\text{-}Bu_2Ph)_2$ is 5035 Hz and for *sym-trans*-$Hg_2Cl_4(P\text{-}n\text{-}Bu_2Ph)_2$ is 7514 Hz)[3] and to changes in coordination number ($^1J(Hg,P)$ for $[Hg(PMe_3)_4](NO_3)_2$ is 2255 Hz and for $[Hg(PMe_3)_3]Cl_2$ is 3580 Hz).[4]

During the preparation of our manuscript a report of the effect of X on the properties of PPh_3 complexes of mercury(II) appeared.[5] Although there is some overlap with our results, these authors assume a tetrahedral geometry for the HgX_2P_2 unit and report no structural data.

Experimental Section

Syntheses. The complexes $HgX_2(PPh_3)_2$ were synthesized by using standard procedures.[6] The elemental analyses and molecular weight determinations (vapor-pressure osmometry) are in agreement with the proposed monomeric composition. Table I contains a summary of the microanalytical data.

^{31}P NMR Measurements. The ^{31}P NMR spectra were obtained on rotating 10-mm tubes on a Bruker-HX90 spectrometer at 36.43 MHz. The solvent was $CDCl_3$ where not otherwise stated. The deuterium frequency of the solvent was used for internal heteronuclear stabilization of the magnetic field. All shifts refer to external H_3PO_4 (85%) at room temperature and are in ppm with a positive sign indicating a low-field (higher frequency) shift. The ^{31}P NMR data are summarized in Table II. For all of the complexes low-temperature measurements were required to obtain the limiting spectra. These spectra were free of additional signals attributable to polymers[3] or impurities.

EHMO Calculations. All calculations were performed with the program WH (Wolfsberg–Helmholz) written by L. Zoller, ETH-Zentrum. The diagonal elements H_{ii} of the Hamiltonian matrix were approximated by the negative valence-shell ionization potentials. The off-diagonal elements H_{ij} were calculated by a weighted Wolfsberg–Helmholz formula[7a] with $k = 1.75$.

Model Calculations on HgB_4^{2-} and $HgA_2C_2^{2-}$. For these calculations the σ donors A^-, B^-, and C^- were represented simply by a Slater 1s orbital with an exponent equal to 1.3. The 5d, 6s, and 6p Slater orbitals on Hg^{2+} and their H_{ii} values are shown in Table III. All mercury–ligand distances were chosen as 1.81 Å (equal to the sum of the covalent radii of Hg and H) with all angles 109.47°. Initially the H_{ii} values of all ligands were placed at −14 eV, in between the mercury d and s levels. Thus HgB_4^{2-} shows T_d symmetry. Subsequently, the effective symmetry was lowered to C_{2v} by increasing the H_{ii}'s of one pair of ligands (C) while decreasing those of the other pair (A) by the same amount. The geometry of the resulting $HgA_2C_2^{2-}$ was kept equal to that of HgB_4^{2-}. Finally, the geometric constraint was relaxed by allowing θ(AHgA) and θ(CHgC) to change in opposite directions but by the same amount.

Model Calculations on $HgCl_2(PH_3)_2$. ζ^2 Slater-type orbitals of Clementi and Roetti[8a] were used to represent the atomic orbitals for phosphorus and chlorine.

For mercury the functions given by Basch et al.[8b] were used. Hydrogen atomic orbitals were represented by a single Slater function with exponent 1.2. The main diagonal elements of the Hamiltonian matrix, H_{ii}, were iterated in self-consistent-charge cycles (SCCC) with use of the quadratic dependence of the ionization potentials on charge as described by Basch et al.[9] The charge dependence of all mercury

* To whom correspondence should be addressed: H.B.B., Laboratorium für Chemische und Mineralogische Kristallographie, Universität Bern, CH-3012 Bern, Switzerland; P.S.P., ETH-Zentrum, CH-8092 Zürich, Switzerland.

(1) D. K. Johnson, P. S. Pregosin, and L. M. Venanzi, *Helv. Chim. Acta*, **59**, 2691 (1976).
(2) M. Barrow, H. B. Bürgi, D. K. Johnson, and L. M. Venanzi, *J. Am. Chem. Soc.*, **98**, 2356 (1976).
(3) (a) S. O. Grim, P. J. Lui, and R. L. Keiter, *Inorg. Chem.*, **13**, 342 (1974); (b) P. L. Goggin, R. J. Goodfellow, D. M. McEwan, and K. Kessler, *Inorg. Chim. Acta*, **44**, L111 (1980).
(4) H. Schmidbaur and K. H. Räthlein, *Chem. Ber.*, **106**, 2491 (1973).
(5) E. C. Alyea, S. A. Dias, R. G. Goel, W. O. Ogini, P. Pilon, and D. W. Meek, *Inorg. Chem.*, **17**, 1697 (1978).
(6) R. C. Evans, F. G. Mann, H. S. Peiser, and D. Purdie, *J. Chem. Soc.*, 1209 (1940).
(7) (a) J. H. Ammeter, H. B. Bürgi, J. C. Thibeault, and R. Hoffmann, *J. Am. Chem. Soc.*, **100**, 3686 (1978); (b) W. Hehre, R. Ditchfield, R. F. Stewart, and J. A. Pople, *J. Chem. Phys.*, **52**, 2769 (1970).
(8) (a) E. Clementi and C. Roetti, *At. Data Nucl. Data Tables*, **14**, 428 (1974); (b) H. Basch and H. B. Gray, *Theor. Chim. Acta*, **4**, 367 (1966).

0020-1669/80/1319-3707$01.00/0

Table I. Analytical Data for the $HgX_2(PPh_3)_2$ Complexes

X	formula	%C calcd	%C found	%H calcd	%H found	%N calcd	%N found	%P calcd	%P found	mp,[a] °C
NO_3	$C_{36}H_{30}HgN_2O_6P_2$	50.92	50.90	3.56	3.64	3.30	3.36	7.29	7.37	192–193
OAc	$C_{40}H_{36}HgO_4P_2$	56.97	54.37	4.30	4.29			7.35	6.94	200 d
Cl	$C_{36}H_{30}Cl_2HgP_2$	54.31	54.43	3.80	3.88					272–273
Br	$C_{36}H_{30}Br_2HgP_2$	48.86	49.10	3.42	3.63					258–259
SCN[b]	$C_{38}H_{30}HgN_2P_2S_2$	54.25	54.10	3.59	3.69	3.33	3.50	7.36	7.53	200–202
I	$C_{36}H_{30}HgI_2P_2$	44.17	44.24	3.09	3.12			6.33	6.49	250 d
CN	$C_{38}H_{30}HgN_2P_2$	58.73	58.55	3.89	3.93	3.60	3.67	7.97	8.11	240 d

[a] d = decomposition. [b] Sulfur analyses: calcd, 7.62; found, 7.59.

Table II. ^{31}P NMR Data for the Mercury–Phosphine Complexes HgX_2P_2

P	X	δ	^1J(Hg,P), Hz	T, K
PPh_3	NO_3	40.4	5925	210
PPh_3	CH_3COO	34.5	5510	220
PPh_3	Cl	28.3	4675	250
PPh_3	Br	21.8	4156	240
PPh_3	SCN	31.3	3725	220
PPh_3	I	1.2	3074	220
PPh_3	CN	17.9	2617	210
$P(m\text{-}CF_3\text{-}C_6H_4)_3$[a]	I	3.7	2922	170
$P(m\text{-}CH_3\text{-}C_6H_4)_3$	I	7.7	3201	220
$PPh_2(CH_2Ph)$	I	11.9	3624	210
P-*n*-Bu_2Ph[b]	I		3726	
P-*n*-Bu_3	I	9.6	4221	220
P-*n*-Et_3	I	20.1	4239	215
P(c-Hx)$_3$	I	37.7	3491	220
PSP[c]	I	−4.5	3420	220
P(c-Hx)$_2$Ph	I	17.7	3689	220

[a] In acetone-d_6. [b] Reference 3. [c] PSP = $(PH_2PCH_2CH_2)_2S$.

Table III. Model Calculations of HgB_4^{2-}: Exponents, Coefficients, and H_{ii} Values of the AO's

AO	ζ (ζ$_2$)	C (C$_2$)	H_{ii}, eV
5d (Hg)	6.436 (3.032)	0.6905 (0.5593)	−18.0
6s (Hg)	2.649	1.0	−10.0
6p (Hg)	2.631	1.0	−5.0

orbitals was assumed to be linear with a slope of 5 eV/charge unit.

SCCC iteration was performed on a molecule with C_{2v} symmetry and the structural parameters d(Hg–P) = 2.47 Å, d(Hg–Cl) = 2.48 Å, d(P–H) = 1.40 Å, and θ(PHgP) = θ(ClHgCl) = θ(HPH) = 110°. The resulting values for H_{ii} and the gross atomic charges Q are

atom	H_{ii}'s of orbitals: s	p	d	gross charge Q
Hg	−10.44	−5.00	−15.66	0.14+
P	−22.19	−12.84		0.26+
Cl	−18.88	−8.39		0.53−
H	−13.89			0.07+

All further calculations on geometrically distorted molecules were performed without further changes of the H_{ii}'s.

After iteration the chlorine 3s- and 3p-orbital energies appear higher than those of the phosphorus orbitals contrary to what is observed for the free atoms. This reversal in relative orbital energies is loosely connected to the partial phosphonium character of coordinated PH_3 and the partial ionic character of coordinated chloride. Thus the chlorine 3s and 3p levels obtained from charge iteration on $HgCl_2(PH_3)_2$ (−18.9 and −8.4 eV) lie energetically higher than those of gaseous, monoatomic chlorine (−29.3 and −13.8 eV),[10a] but lower than those of Cl^- in NaCl(s) (−16 and −5 eV).[10a] A further comparison can be made between the 3p levels of Cl^- in $HgCl_2(PH_3)_2$ and the ionization energies of the $^2\pi_g$ and $^2\pi_u$ MO's in $HgCl_2$(g) (11.5 and 12.2 eV),[10b] which are composed mostly of nonbonding chlorine 3p orbitals. Their energies are similar and lie in between Cl(g) and NaCl(s). Similarly, the ionization energies of the mercury 5d electrons in $HgCl_2$(g) (16.5 and 19.0 eV) are comparable to the energies of the d-block MO's of $HgCl_2(PH_3)_2$ (between 15.5 and 16 eV).[10b]

Analogous comparisons for the PH_3 ligand orbitals in $HgCl_2(Ph_3)_2$ are more difficult to obtain since no comparable ionization energies are available. However, ab initio calculations for PH_3, H_3BPH_3, and PH_4^+ have been performed with the help of the GAUSSIAN-70 program[11] with use of an STO-3G basis set of atomic orbitals and experimental molecular geometries. The PH_3 group orbital, which is composed mainly of phosphorus 3s and hydrogen 1s AO's, was calculated at −23.7, −25.8, and −32.6 eV, respectively. The two PH_3 group orbitals composed of phosphorus 3p and hydrogen 1s have calculated energies of −14.1, −16.0, and −22.6 eV, respectively. The intermediate energies calculated for the borane complex agree with the corresponding energies in $HgCl_2(PH_3)_2$ (ca. −25.3 and −16.5 eV) obtained through SCCC–EHMO calculations.

The consequences of the agreement between experimental or ab initio energies, on the one hand, and SCCC-EHMO energies on the other hand, should not be overrated, since the validity of our calculations as far as coupling constants are concerned depends more on the form of the MO's and in particular on the coefficients of the s-type AO's.

Results and Discussions

Table II shows ^{31}P chemical shifts, δ, and ^{31}P–^{199}Hg coupling constants, ^1J(Hg,P), for the mercury(II)–phosphine complexes $HgX_2(PPh_3)_2$, X = NO_3, CH_3COO, Cl, Br, SCN, I, and CN, and HgI_2P_2, P = $P(m\text{-}CF_3C_6H_4)_3$, PPh_3, $(Ph_2PCH_2CH_2)_2S$, $PPh_2(CH_2Ph)$, P-*n*-Bu_2Ph, P-*n*-Bu_3, and P(c-Hx)$_3$. The most obvious feature displayed by these data is the marked change in ^1J(Hg,P) as a function of the anion X and—to a lesser extent—the phosphine P. The complex $Hg(NO_3)_2(PPh_3)_2$ shows a coupling constant of 5925 Hz, the largest in this series, whereas ^1J(Hg,P) for $Hg(CN)_2(PPh_3)_2$ is 2617 Hz and represents the smallest in this series. For the linear mercury complexes RHgX (with X = the above anions and R = CH_3, $CH_3OC(CH_3)_2CH_2$) a similar dependence of both the one- and two-bond coupling constants $^1J(^{199}Hg,^{13}C)$[12a] and $^2J(^{199}Hg,^1H)$[12b] on the nature of X has been described.

In order to illustrate the similarity of the NMR data for these two families of mercury complexes, we compare, in Figure 1, ^1J(Hg,P) for $HgX_2(PPh_3)_2$ with both ^1J(Hg,C) and ^2J(Hg,H) for RHgX with R = $CH_3OC(CH_3)CH_2$. Both scatter plots show a reasonable linear correlation (r^2 = 0.96 and 0.97). This suggests a characteristic property of the anion X which affects all three coupling constants in a similar way; however, the changes in ^1J(Hg,P) relative to the changes in either ^1J(Hg,C) or ^2J(Hg,H) are larger by approximately a factor of 2. Thus $^1J(Hg,P)_{NO_3}/^1J(Hg,P)_{CN}$ = 2.26, whereas

(9) H. Basch, A. Viste, and H. B. Gray, *Theor. Chim. Acta*, **3**, 458 (1965).
(10) (a) K. Siegbahn, *Pure Appl. Chem.*, **48**, 77 (1976); (b) J. Berkowitz, *J. Chem. Phys.*, **61**, 407 (1974).
(11) The ab initio program used was GAUSSIAN-70, Quantum Chemistry Program Exchange, Indiana University, No. 236. The STO-3G basis set is described in ref 7b. The geometries used were as follows: for PH_3, HPH = 93.8°, r(P,H) = 1.4206 Å; for PH_4^+, r(P,H) = 1.414 Å; for H_3B–PH_3, PBH = 103.6°, BPH = 116.9° (staggered), r(B,H) = 1.212 Å, r(P,H) = 1.399 Å, r(B,P) = 1.937 Å.
(12) (a) G. Singh, *J. Organomet. Chem.*, **99**, 251 (1975); (b) T. Iwayanagi, T. Ibusiki, and Y. Saito, *ibid.*, **128**, 145 (1977).

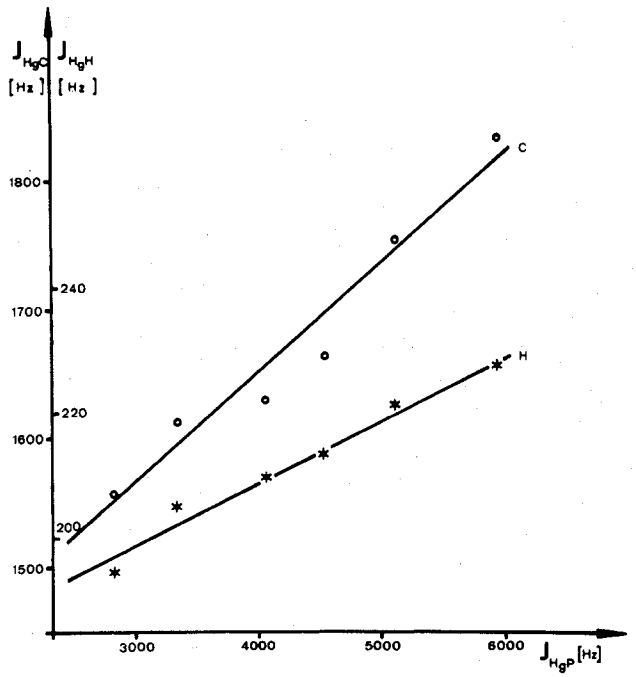

Figure 1. Plot of the coupling constants $^1J(Hg,C)$ and $^2J(Hg,H)$ in $HgX(CH_2C(OMe)Me_2)$ vs. $^1J(Hg,P)$ in $HgX_2(PPh_3)_2$, X = CN^-, I^-, SCN^-, Br^-, Cl^-, and CH_3COO^-.

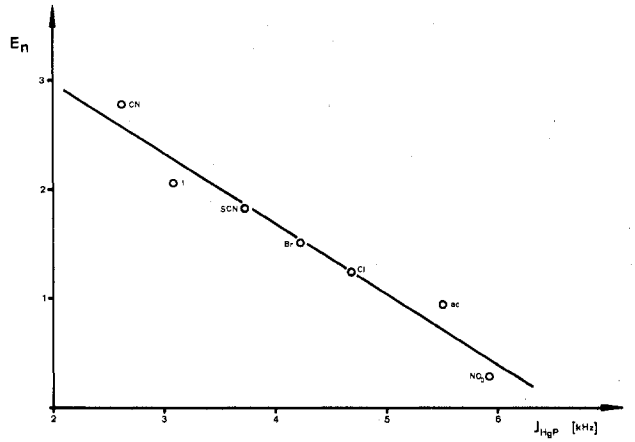

Figure 2. Plot of the coupling constant $^1d(Hg,P)$ in $HgX_2(PPh_3)_2$ vs. the nucleophilicity parameter E_n.

the corresponding ratios involving $^1J(Hg,C)$ and $^2J(Hg,H)$ are less than 1.3. Therefore, although the various mercury–ligand couplings are related, it seems that significant differences exist as well.

Data are also available for $^1J(^{195}Pt,^{31}P)$ in the complexes *trans*-$PtX_2(P\text{-}n\text{-}Bu)_2$.[13a] For these compounds the one-bond coupling constants vary from 2158 (X = CN) to 2506 Hz (X = ONO_2). This ratio (1.16) is also considerably smaller than found for the mercury–phosphine system. The ratio observed for $^1J(Pt,P)$ in *trans*-$PtHX(PPh_3)_2$ compounds is similarly small.[13b] Even for the molecules *cis*-$PtX_2(P\text{-}n\text{-}Bu_3)_2$, where the X ligand lies trans to phosphorus, that is, where one can invoke the *trans-influence concept*, the quotient $^1J(Pt,P)_{NO_3}/^1J(Pt,P)_{CN}$ is 1.38, which is still considerably smaller than 2.26.

For a discussion of the dependence of coupling constants on the chemical nature of X, we have chosen to use the empirical measure of nucleophilicity E_n proposed by Edwards.[14] The correlation between E_n and $^1J(Hg,P)$ (Figure 2) is approximately linear and suggests that for poor electron donors X the coupling constants between the mercury and phosphorus atoms will be larger than those for the good electron donors. We also attempted to correlate $^1J(Hg,P)$ with the equilibrium constants log β_4[15] for the reaction $Hg^{2+}(H_2O)_n + 4X \rightleftarrows Hg^{2+}X_4 + H_2O$. The general trend is the same as that observed for the correlation with E_n, but the deviations from linearity are more pronounced. We find, therefore, that our NMR data can be related to several different physicochemical parameters.

Table IV. Coordination Geometry of Hg^{2+} in $HgX_2(PPh_3)_2$[a]

X	⟨*d*(HgP)⟩	⟨*d*(HgX)⟩	θ(PHgP)	θ(XHgX)
NO_3^- [d]	2.451 (1)	2.507 (4)	131.8 (1)	70.0 (2)
SCN^- [b]	2.488 (3)	2.571 (3)	118.1 (1)	96.7 (1)
I^- [c]	2.566 (3)	2.748 (1)	109.0 (1)	110.4 (1)
CN^- [d]	2.515 (7)	2.234 (26)	108.9 (2)	108.5 (15)

[a] The X-ray diffraction data are averaged to correspond to C_{2v} symmetry. Esd's in units of least significant figure are in parentheses. [b] Data from ref 17b. [c] Data from ref 17a. [d] See ref 25a.

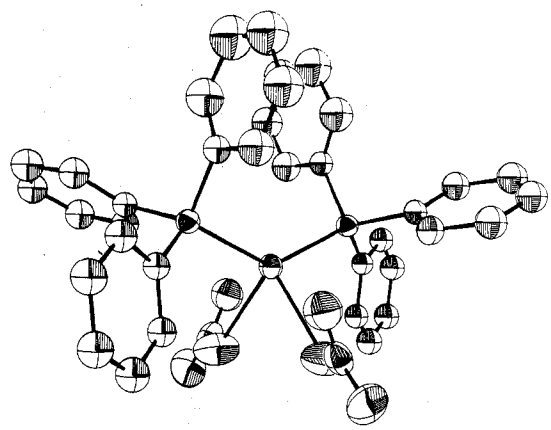

Figure 3. ORTEP plot of $Hg(NO_3)_2(PPh_3)_2$.

The varying nature of X in the complexes $HgX_2(PPh_3)_2$ is not only reflected in the variation of $^1J(Hg,P)$ but also in their molecular structures as determined from X-ray diffraction experiments on the crystalline solids. Table IV lists averaged bond lengths and bond angles of the distorted mercury coordination tetrahedra for the complexes $HgX_2(PPh_3)_2$ (X = NO_3,[16a] SCN, I, CN), and Figure 3 shows an ORTEP plot for the dinitrate complex. The angle θ(PHgP) decreases from ~132° in the nitrate salt to ~109° in the iodide and cyanide salts. At the same time θ(XHgX) increases from ~70 to ~110°. The lower limit for θ(PHgP) may be estimated[16b] to be ~95° and is probably dictated by the steric requirements of PPh_3, whereas the lower limit for θ(XHgX) seems to depend mainly on the van der Waals radius (size) of the anion. The angle changes are accompanied by changes in the Hg–P distances, which increase from 2.45 in the nitrate to 2.56 Å in the iodide.[17a] The correlation between change in bond

(13) (a) G. G. Mather, G. J. N. Rapsey, and A. Pidcock, *Inorg. Nucl. Chem. Lett.*, **9**, 567 (1973); (b) G. Socrates, *J. Inorg. Nucl. Chem.*, **31**, 1667 (1969).

(14) J. O. Edwards, *J. Am. Chem. Soc.*, **76**, 1540 (1954).

(15) J. Bjerrum, *Chem. Rev.*, **46**, 381 (1950).

(16) (a) An alternative way of looking at the coordination sphere of this compound is in terms of a bicapped tetrahedron in which oxygen atoms of the nitrate do the capping. These atoms are 2.790 (4) Å from Hg^{2+}; (b) This estimation is based on literature data. See, for example, F. Cariati, R. Mason, G. B. Robertson, and R. Ugo, *Chem. Commun.*, 408 (1967); J. Howard and P. Woodward, *J. Chem. Soc., Dalton Trans.*, 1840 (1973); D. R. Russell and P. A. Tucker, *ibid.*, 2222 (1975); S. Bhaduri, B. F. G. Johnson, A. Pidcock, P. Taithby, G. Sheldrick, and C. I. Zuccaro, *J. Chem. Soc., Chem. Commun.*, 354 (1977).

angles and distances, as observed here, is similar to that described elsewhere for tetrahedral $AlCl_4$, PO_4, and SO_4 fragments.[18]

The structural data may be discussed more coherently and in more detail in terms of molecular orbital (MO) theory. Specifically for the model molecule MB_4^{2-}, we have investigated the effects on structure of replacing the ligands, B, by a pair of poorer σ donors, A, and a pair of better σ donors, C, to yield $MA_2C_2^{2-}$.

The MO's of the T_d symmetric MB_4^{2-} species can be classified as follows: $1t_2$ (d_{xz}, d_{yz}, d_{xy}, ligand; bonding), 1e (d_{x^2}, $d_{x^2-y^2}$), $1a_1$ (s, ligand; bonding), $2t_2$ (d_{xz}, d_{yz}, d_{xy}, ligand; antibonding); p_x, p_y, p_z, ligand; bonding), all occupied, and $2a_1$ (s, ligand; antibonding), $3t_2$ (p_x, p_y, p_z, ligand; antibonding), both empty. In going from MB_4^{2-} to $MA_2C_2^{2-}$ the geometry was initially kept unchanged; nevertheless, the symmetry is lowered to C_{2v} due to the unsymmetrical substitution. The orbitals are now 1a (d_{xy}, s, ligand A; bonding), $1b_2$ (d_{yz}, ligand A; bonding), $1b_1$ (d_{xz}), $1a_2$ ($d_{x^2-y^2}$), $2a_1$ (d_{z^2}), $3a_1$ (d_{xy}, s, ligand; nonbonding), $2b_2$ (d_{yz}, p_y, ligand; nonbonding), $4a_1$ (s, p_z, ligand C; bonding) and $2b_1$ (p_x, ligand C; bonding). The redistribution of electron density is accompanied by a change in the total overlap populations (OP). MA shows a lower while MC shows a higher overlap population than MB. To the extent that a higher OP indicates an increase in bond strength and a decrease in bond lengths, we may compare the calculated result with the experimentally determined distances in $HgI_2(PPh_3)_2$ and $Hg(NO_3)_2(PPh_3)_2$: for the combination of a very poor σ donor, NO_3^-, and a good σ donor, PPh_3, the distance Hg–P is 2.45 Å, 0.1 Å shorter than for the combination of two good σ donors, I^- and PPh_3, where the Hg–P distance is 2.56 Å. In addition, it might be expected that the lowering of the symmetry brought about by changing MB_4^{2-} into $MA_2C_2^{2-}$ leads to a change in angles. Variation of the angles with the constraint $\theta(AMA) + \theta(CMC) = 220°$ leads to an equilibrium structure with $\theta(AMA) < \theta(CMC)$ but with only slightly lower energy ($\lesssim$1 kcal mol^{-1}). This calculated result, namely, that the larger angle is found between the better σ donors, is paralleled by the observed structures of $Hg(PPh_3)_2X_2$ (X = NO_3, NCS, I, CN), where θ(XHgX) decreases and θ(PHgP) increases with the decreasing σ-donating capability of X.

The data in Table IV show not only correlated changes in θ(PMP) and θ(XMX) but also an increase of the distance r(Hg–P) with decreasing angle θ(PHgP). To obtain further insight into this correlation, we have performed an EH calculation on $HgCl_2(PH_3)_2$ holding the sum θ(PHgP) + θ(ClHgCl) at 220°. We find that an increase in the ligand–mercury–ligand angle leads to an increase in the metal–ligand overlap population, i.e., to stronger bonding and presumably shorter bond lengths as observed experimentally.

The spectroscopic and structural findings are combined in Figure 4, which shows the dependence of ^1J(Hg,P) on θ(PHgP), θ(XHgX), and r(Hg–P), respectively. As the Hg–X bonding changes from more ionic (NO_3^-) to more covalent (CN^-), ^1J(Hg,P) decreases, θ(PHgP) decreases, θ(XHgX) increases, and r(Hg–P) increases. In order to appreciate the connection between the NMR and X-ray data, it is useful to recall the factors affecting one-bond coupling constants. This is conveniently done by analyzing, as a first approximation, the correlation between ^1J(Hg,P) and θ(PHgP) in terms of

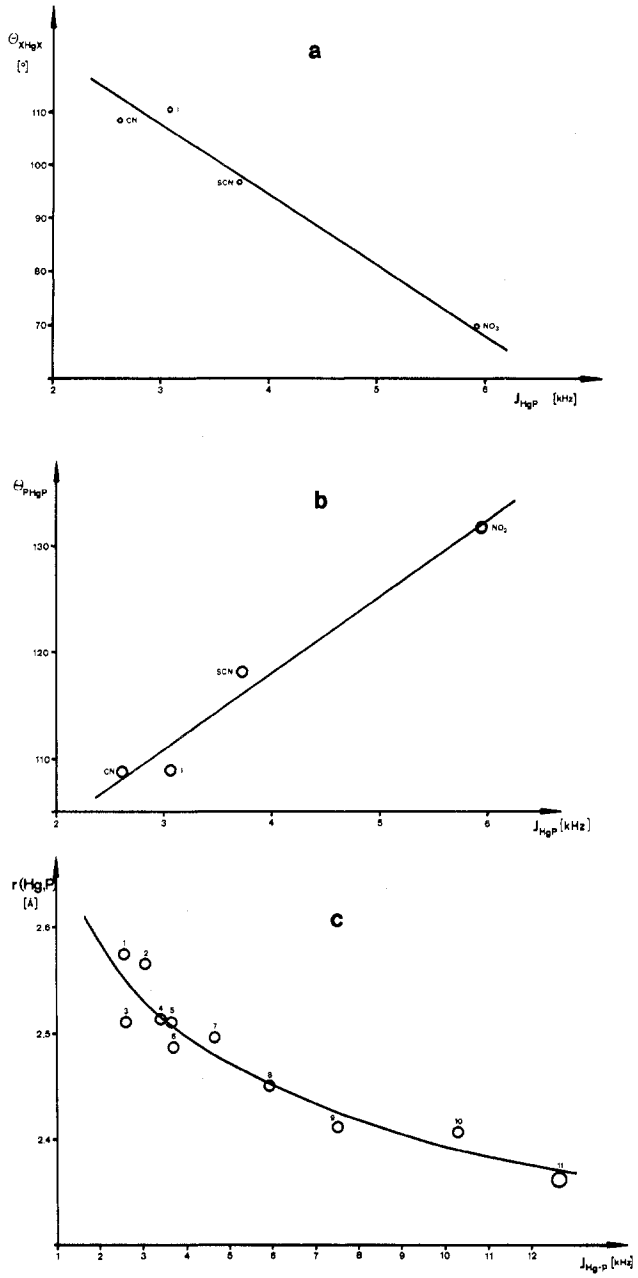

Figure 4. Dependence of ^1J(Hg,P) in $HgX_2(PPh_3)_2$ on the following structural parameters (X = CN^-, I^-, SCN^-, NO_3^-): (a) correlation of ^1J(Hg,P) with θ(PHgP), (b) correlation of ^1J(Hg,P) with θ(XHgX), (c) correlation of ^1J(Hg,P) with r(Hg,P). Key: 1, $HgBr_2$(dppet);[25a] 2, $HgI_2(PPh_3)_2$;[17a] 3, $Hg(CN)_2(PPh_3)_2$;[25a] 4, HgI_2(PSP);[25b] 5, HgI_2(PP);[25d] 6, $Hg(SCN)_2(PPh_3)_2$;[17b] 7, $HgCl_2$(PP);[25d] 8, $Hg(NO_3)_2(PPh_3)_2$;[25a] 9, Hg[P(O)(OEt)$_2$]$_2$;[24] 10, [$Hg(NO_3)_2$(Pmesityl$_3$)]$_2$;[25c] 11, HgCl[P(O)(OEt)$_2$].[24]

an oversimplified hybridization model which assumes that changes in the Fermi contact term[21a] dominate changes in ^1J(Hg,P), as shown in eq 1, where α_{Hg}^2 and α_P^2 are the s characters of the hybrid orbitals used to form the Hg–P bond, $|\psi_{ns}(0)|^2$ is the valence s-electron density at the nucleus, and ΔE is the mean triplet excitation energy.

$$^1J(\mathrm{Hg,P}) \propto \alpha_{Hg}^2\alpha_P^2|\psi_{6s}(0)_{Hg}|^2|\psi_{3s}(0)_P|^2/\Delta E \qquad (1)$$

(17) (a) L. Fälth, *Chem. Scr.*, **9**, 71 (1976); (b) R. C. Nakhija, A. L. Beauchamp, and R. Divest, *J. Chem. Soc., Dalton Trans.*, 2447 (1973).
(18) P. Murray-Rust, H. B. Bürgi, and J. D. Dunitz, *Acta Crystallogr., Sect. B*, **B34**, 1793 (1978).
(19) J. A. Pople and D. P. Santry, *Mol. Phys.*, **8**, 1 (1964).
(20) Analysis of the individual orbital energies as a function of bond angles shows only small changes in energy with levels often running parallel to one another.
(21) (a) E. F. Mooney, *Annu. Rev. NMR Spectrosc.*, **1** (1968); **2** (1969); E. F. Mooney, *Annu. Rep. NMR Spectrosc.*, **3–7** (1970–1977); (b) P. S. Pregosin and R. W. Kunz, "NMR, Principles and Progress", Vol. 16, Springer-Verlag, New York, 1979. R. W. Kunz, *Helv. Chim. Acta*, in press.

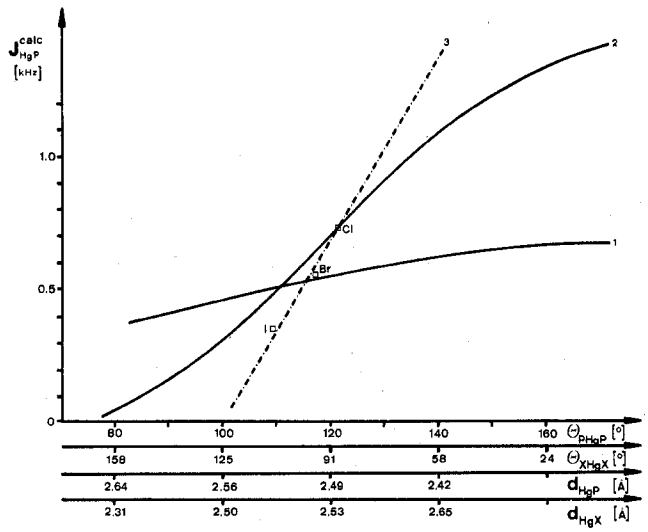

Figure 5. Plot of J(Hg,P), calculated for $HgX_2(PH_3)_2$, as a function of the structural parameters r and θ and of the anion X. (1) X = Cl; the bond lengths l(Hg,P) and l(Hg,Cl) are varied in opposite directions. The bond length combinations used are given on the lower two scales. (Distance scales are not linear!) PHgP = XHgX = 110°. (2) X = Cl (additional variation of θ(PHgP) and θ(XHgX)). The geometry of $HgCl_2(PH_3)_2$ at any point is given by a consideration of all four scales. (3) Chlorine is replaced at different geometries by the appropriate anions (Cl, Br, I).

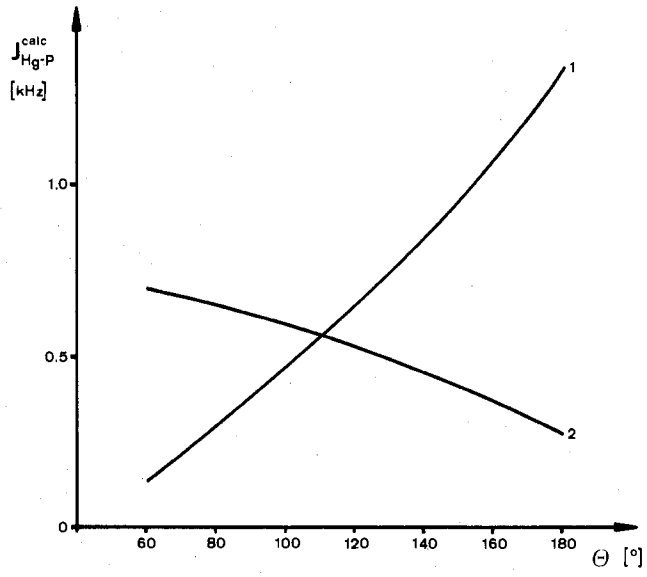

Figure 6. Plot of $^1J(Hg,P)_{calcd}$ vs. (1) θ(XHgX) with the constraint θ(PHgP) = 110° and (2) θ(PHgP) with the constraint θ(XHgX) = 110°. The bond lengths are constant at l(Hg,P) = 2.48 Å and l(Hg,Cl) = 2.47 Å.

It is generally accepted[21b] that the terms $|\psi_{rs}(0)|^2$ and ΔE do not change significantly for a related series of molecules. Although this approximation may not be generally valid, at this stage, we will assume, as others have done, that the hybridization terms dominate the changes in the coupling constants. Within this framework we can use the bond angles at Hg and P as an approximate measure of the α^2 terms.[22] The average CPC or HgPC angles in the four compounds for which X-ray structures are available span a range of only 2°.[23] We therefore feel justified in assuming that α_P^2 is essentially the same in all four compounds. For mercury, on the other hand, the PHgP bond angles cover a range of 23° (109–132°). We relate this to the change in s character of four tetrahedrally disposed, C_{2v} symmetric hybrid orbitals on Hg^{2+} built from the 6s- and 6p-valence orbitals. These hybrid orbitals are specified by fixing one angle between equivalent hybrids, e.g., θ(PHgP). θ(XHgX) and the s character of all orbitals involved are then determined via symmetry and orthogonality conditions. For the angles θ(PHgP) given in Table IV we estimate α_{Hg}^2 to be 0.40, 0.32, 0.25, and 0.24, respectively. Comparison of these numbers with the coupling constants in Table II reveals that an increase in α_{Hg}^2 is paralleled, if only crudely, by an increase in the observed ^1J(Hg,P). Thus an increase in θ(PHgP) may be qualitatively associated with an increase in ^1J(Hg,P).

In order to refine our understanding of the coupling constant data and their dependence on molecular and electronic structure, we have considered the Fermi contact term in the somewhat more detailed form developed by Pople and Santry[19] (eq 2). In this equation the mean triplet-energy approximation

$$^1J(A,B) \propto |\psi_{s,A}(0)|^2|\psi_{s,B}(0)|^2\pi_{A,B} \qquad (2)$$

$$\pi_{A,B} = 4\sum_{i}^{occ}\sum_{j}^{unocc}(^3\Delta E_{i,j})^{-1}C_{i,A}C_{j,A}C_{i,B}C_{j,B} = 4\sum_{i}\sum_{j}\prod_{i\to j}$$

is rejected and the polarizability term $\pi_{Hg,P}$, which replaces $\alpha_P^2\alpha_{Hg}^2/\Delta E$ in eq 1, is calculated on the basis of EHMO calculations as described in the Experimental Section.[20] We analyzed changes in coupling constants in terms of contributions from changes in bond angles, bond distances, and anions or some combination of these. Calculations have been performed on $HgX_2(PH_3)_2$ (X = Cl, Br, I), taking into account various structural changes (see Experimental Section). Results are shown in Figure 5 for (1) simultaneous changes in the Hg–P and Hg–X distances with constant bond angles and anions, (2) simultaneous changes in the bond angles θ(XHgX) and θ(PHgP) and bond distances with constant anion, and (3) simultaneous changes of distances, angles, and anion. The most interesting points to be noted are as follows: (1) curve 1 has a relatively small slope, suggesting that increasing the Hg–X distance while decreasing the Hg–P distance results in only small changes in ^1J(Hg,P), and (2) curves 2 and 3 are markedly steeper; i.e., changes in the bond angles and anions X affect ^1J(Hg,P) much more. We have analyzed this phenomenon somewhat further. In Figure 6 we report results for the molecule $HgCl_2(PH_3)_2$ for different angular distortions. We find that for a fixed θ(XHgX) of 110°, the slope of θ(PHgP) vs. ^1J(Hg,P) is much steeper than that of θ(XHgX) vs. ^1J(Hg,P) with θ(PHgP) fixed at 110°. Taken together with Figure 5 this means that the anion X and the PHgP angle make the major contributions to the changes in the values of ^1J(Hg,P). The effect of changes in the PHgP angle on ^1J(Hg,P), as predicted by the extended Hückel calculations, explains the observation that the experimentally obtained ratio $^1J(Hg,P)_{NO_3}/^1J(Hg,P)_{CN}$ is 2.26 for the tetrahedral mercury complexes but only 1.15 for the linear molecules HgX(PO(OEt)$_2$)$_2$[24] for which an analogous angular distortion is not possible. Similar arguments might be applicable also for the dependence of metal–ligand coupling constants on the geometry of tetrahedral complexes of Cd(II), Ag(I), and Pt(0) and

(22) L. Pauling in "The Nature of the Chemical Bond", Cornell University Press, Ithaca, NY, 1960.
(23) H. B. Bürgi, R. W. Kunz, and P. S. Pregosin, unpublished results, as well as ref 17.
(24) J. Bennett, A. Pidcock, C. R. Waterhouse, P. Coggon, and A. T. McPhail, *J. Chem. Soc. A*, 2094 (1970).
(25) (a) H. B. Bürgi, R. W. Kunz, M. Parvez, and P. S. Pregosin, unpublished results (dppet = *cis*-bis(diphenylphosphino)ethene); (b) K. Aurivillius and L. Fälth, *Chem. Scr.*, 4, 215 (1973) (PSP = bis(diphenylphosphino)ethylene sulfide); (c) E. C. Alyea, S. A. Dias, G. Ferguson, and M. Parvez, *Inorg. Chim. Acta*, 37, 45 (1979); (d) R. W. Kunz, P. S. Pregosin, and L. Zambonelli, unpublished results (PP = 2,11-bis((diphenylphosphino)methyl)benzo[*c*]phenanthrene).

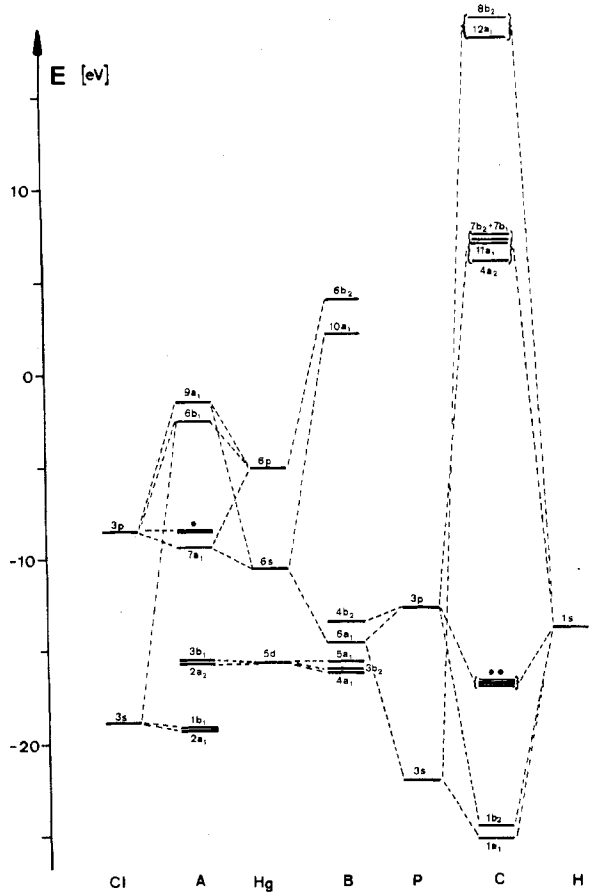

Figure 7. MO diagram of $[HgCl_2(PH_3)_2]$: A, MO's localized mainly between Hg and Cl; B, MO's localized mainly between Hg and P; C, MO's localized mainly between P and H. The separation of the MO's into three groups does not mean that the orbitals were localized; they are still canonical (*, $8a_1 + 3a_2 + 4b_1 + 5b_1 + 5b_2$; **, $3a_1 + 1a_2 + 2b_1 + 2b_2$).

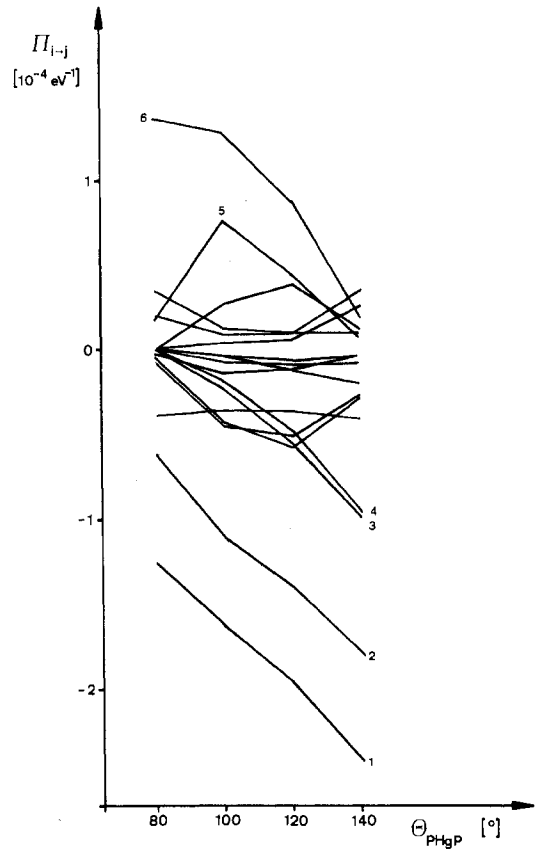

Figure 8. Plot of the contributions to the double sum in eq 2 vs. θ(PHgP). The actual geometry at each angle is that of curve 2 in Figure 5. Only contributions greater than 10^{-5} eV^{-1} are included. The labeled contributions belong to the following transitions: 1, $1a_1 \rightarrow 12a_1$; 2, $6a_1 \rightarrow 12a_1$; 3, $1a_1 \rightarrow 10a_1$; 4, $6a_1 \rightarrow 10a_1$; 5, $7a_1 \rightarrow 10a_1$; 6, $7a_1 \rightarrow 12a_1$.

of trigonal complexes of Ag(I).

We have also analyzed the contribution of the individual MO's to $\pi_{Hg,P}$. Figure 7 shows that for $HgCl_2(PH_3)_2$ there are 12 a_1-type MO's (8 occupied and 4 unoccupied), all of which may contribute to the polarizability term. Of the 32 individual transitions from occupied to unoccupied MO's, 17 contribute more than 10^{-5} eV^{-1} to the polarizability ($10^{-3} < \pi_{Hg,P} < 3 \times 10^{-2}$, see Figure 8), and of these, 6 are major contributors and determine the variation of $\pi_{Hg,P}$ as a function of geometry. The latter transitions arise from three ($1a_1$, $6a_1$, and $7a_1$) filled and two ($10a_1$ and $12a_1$) empty orbitals. The orbital $1a_1$ is mainly P–H bonding with a small bonding admixture of 6s on Hg; $6a_1$ is essentially Hg–P bonding (comparable to the orbital in $MA_2C_2^{2-}$ which is (d_{xy}, s, ligand; bonding); $7a_1$ is Hg–Cl bonding, comparable to the orbital in $MA_2C_2^{2-}$ which is (s, p_z, ligand C; bonding). The importance of contributions to $\pi_{Hg,P}$ from transitions involving the MO's $1a_1$ and $6a_1$ can be gauged from the experimental data with the help of a simple qualitative argument: a change in the R group of the phosphorus ligand P will affect the nature of the P–R bond and, as a consequence, the nature of the P lone pair and therefore the P–Hg bond. The effects of varying the hydrocarbon substituent on ^1J(Hg,P) are shown in Table II for the iodide complexes HgI_2P_2.

Finally it may be noted that the MO's $6a_1$ and $7a_1$ are also responsible for Hg–P and Hg–Cl bonding and that they depend markedly on geometry. They contribute about one-third to the total overlap population for all geometries considered, and thus they reflect the trends in overall bonding. The computational result that the MO's $6a_1$ and $7a_1$ are substantially involved in both determining structure and coupling constants provides a theoretical framework for the empirical correlation of NMR data in solution with the structural data in the solid state. It thus becomes possible to establish a relationship between θ(PHgP) or, to a lesser extent, θ(XHgX) and the ^1J(Hg,P) coupling constants and to test this relationship by using specifically designed molecules containing different combinations of PHgP and XHgX angles. Studies along these lines are being undertaken with the help of chelating diphosphine ligands imposing various constraints on the geometry of the corresponding complexes.

Acknowledgment. We thank the Swiss National Science Foundation for support (R.W.K.), Mr. L. Zoller for computational assistance, and Mr. E. Fischer for help in the crystal structure determinations.

Registry No. $Hg(NO_3)_2(PPh_3)_2$, 14057-00-2; $Hg(CH_3COO)_2(PPh_3)_2$, 66119-73-1; $HgCl_2(PPh_3)_2$, 14494-85-0; $HgBr_2(PPh_3)_2$, 14586-76-6; $Hg(SCN)_2(PPh_3)_2$, 27290-69-3; $HgI_2(PPh_3)_2$, 14494-95-2; $Hg(CN)_2(PPh_3)_2$, 27902-66-5; $HgI_2[P(m\text{-}CF_3\text{-}C_6H_4)_3]_2$, 74854-36-7; $HgI_2[P(m\text{-}CH_3\text{-}C_6H_4)_3]_2$, 74854-37-8; $HgI_2[PPh_2(CH_2Ph)]_2$, 74854-33-4; $HgI_2[P\text{-}n\text{-}Bu_2Ph]_2$, 43112-08-9; $HgI_2[P\text{-}n\text{-}Bu_3]_2$, 41665-93-4; $HgI_2[PEt_3]_2$, 74854-34-5; $HgI_2[P(c\text{-}Hx)_3]_2$, 50725-85-4; HgI_2[PSP], 51404-87-6; $HgI_2[P(c\text{-}Hx)_2Ph]_2$, 74854-35-6.